buildings

MDPI

Article

The Influence and Mechanism of Polyvinyl Alcohol Fiber on the Mechanical Properties and Durability of High-Performance Shotcrete

Ge Zhang [1,2], Like Li [1,2], Huawei Shi [1,2], Chen Chen [1,2] and Kunpeng Li [1,2,*]

[1] Yellow River Institute of Hydraulic Research, Yellow River Water Conservancy Commission, Zhengzhou 450003, China; gezhangyrihr@163.com (G.Z.); hkylilike@126.com (L.L.); 15538352232@163.com (H.S.); 15617633649@163.com (C.C.)
[2] Key Laboratory of Lower Yellow River Channel and Estuary Regulation, Ministry of Water Resources, Zhengzhou 450003, China
* Correspondence: likunpeng@hky.yrcc.gov.cn

Abstract: This study investigates the impact of polyvinyl alcohol (PVA) fibers on the mechanical properties and durability of high-performance shotcrete (HPS). Results demonstrate that PVA fibers have a dual impact on the performance of HPS. Positively, PVA fibers enhance the tensile strength and toughness of shotcrete due to their intrinsic high tensile strength and fiber-bridging effect, which significantly improves the material's splitting tensile strength, deformation resistance, and toughness, and the splitting tensile strength and peak strain have been found to be increased by up to 30.77% and 31.51%, respectively. On the other hand, the random distribution and potential agglomeration of PVA fibers within the HPS matrix can lead to increased air-void formations. This phenomenon raises the volume content of large bubbles and increases the average bubble area and diameter, thereby elevating the pore volume fraction within the 500–1200 μm and >1200 μm ranges. Therefore, these microstructural changes reduce the compactness of the HPS matrix, resulting in a decrease in compressive strength and elastic modulus. The compressive strength exhibited a reduction ranging from 10.44% to 15.11%, while the elastic modulus showed a decrease of between 8.09% and 12.67%. Overall, the PVA-HPS mixtures with different mix proportions demonstrated excellent frost resistance, chloride ion penetration resistance, and carbonation resistance. The electrical charge passed ranged from 133 to 370 C, and the carbonation depth varied between 2.04 and 6.12 mm. Although the incorporation of PVA fibers reduced the permeability and carbonation resistance of shotcrete, it significantly mitigated the loss of tensile strength during freeze–thaw cycles. The findings offer insights into optimizing the use of PVA fibers in HPS applications, balancing enhancements in tensile properties with potential impacts on compressive performance.

Keywords: polyvinyl alcohol fiber; high-performance shotcrete (HPS); mechanical properties; durability; microstructure

Citation: Zhang, G.; Li, L.; Shi, H.; Chen, C.; Li, K. The Influence and Mechanism of Polyvinyl Alcohol Fiber on the Mechanical Properties and Durability of High-Performance Shotcrete. *Buildings* **2024**, *14*, 3200. https://doi.org/10.3390/buildings14103200

Academic Editor: Dan Bompa

Received: 14 August 2024
Revised: 29 September 2024
Accepted: 4 October 2024
Published: 8 October 2024

1. Introduction

Concrete is one of the most widely used construction materials due to its versatility and strength [1,2], but it also features limitations such as susceptibility to cracking and the need for extensive formwork [3,4]. To address these challenges, researchers have developed advanced materials [5,6], such as shotcrete, which offers rapid application and enhanced durability. Shotcrete is a versatile construction material that is being increasingly used in projects that require rapid application and high strength. This specialized form of concrete is conveyed through an inflated pipeline using compressed air or other power sources and is sprayed at high speed onto a surface to form a solid structure [7]. Compared to ordinary concrete, shotcrete can be directly formed by relying on the receiving surface [8], offering significant advantages such as a short setting time, high early strength, and ease

of construction [9]. These properties make shotcrete ideal for engineering applications like tunnel linings, mine shaft support, slope stabilization, repair works, and protective structures, and it is widely used in engineering fields for elements such as tunnel structures, mine shaft support, slope engineering, repair works, and protective works [10,11].

With the rapid expansion of infrastructure projects in China and around the world, the demand for shotcrete has increased significantly. At the same time, there is a growing need for enhanced performance, leading to the development of high-performance shotcrete (HPS) [12]. HPS is characterized by its excellent workability [13], high strength [14], and durability, which make it suitable for challenging construction environments [15,16]. The excellent workability of HPS helps it maintain a low rebound rate and a certain build-up thickness while in spray form, enabling the shotcrete to have a high level of compactness. The higher strength allows the shotcrete to have a higher-level stiffness to better limit the deformation of surrounding rock in complex sections, and its excellent durability meets the requirements of structural service life in complex service environments. Notable applications of HPS include the Kunming–Shijiazhuang expressway, Wushaoling Tunnel, Jiaozhou Bay Subsea Tunnel, and the Bailianhe Pumped Storage Power Station. For instance, He Shaohui implemented a 30 m-long C45 wet-sprayed fiber high-performance concrete single-layer permanent lining in the Xiaotuanshan tunnel, achieving remarkable results [17].

In order to improve the long-term properties of concrete, such as strength and durability in different environments, various fibers have been widely used which may have a beneficial or adverse effects on concrete properties. Polypropylene (PP) [18], polyamide (PA), steel (ST) [19], forta ferro (FF) and glass (GL) fibers are typically incorporated [20,21].

Different fibers have impact on the workability, strength, and toughness properties of wet-mix shotcrete. In terms of workability, it has been observed that all the fibers affected the workability of fresh concrete quite negatively. The most important reason for the decrease in workability properties of shotcrete mixes is the occurrence of agglomeration with increasing fiber amounts. In addition, fibers absorb moisture from the concrete mixture during the mixing process, thereby reducing the flowability of the mixture [22–24]. Monson L et al. found that, when the fiber content increases from 0.25% to 1.0%, the flowability of mixtures containing PA, FF, and ST fibers significantly decreases, going from 110 mm to 25 mm, 37 mm, and 44 mm, respectively. Compared to ST, the flowability of mixtures containing PA and FF fibers is even lower. It is clearly seen that the use of a fiber volumetric ratio above 1% will be quite inconvenient in terms of the workability of shotcrete mixes. Therefore, it is recommended that the fiber content should not exceed 1.0% [25]. Jiaqing Wang et al. found that the slump was reduced by introducing more fibers [26]. As expected, the air void content increased with the added fibers in concrete mixes. Since the added PVA fibers can increase the viscosity of the fresh matrix and reduce the workability, more entrapped air bubbles remained inside rather than escaping to the surface at the fresh stage [27].

In terms of mechanical properties, polypropylene fibers, for example, have been shown to improve splitting tensile strength and reduce water permeability. Steel fibers are highly effective in increasing strength and toughness, while glass fibers help prevent cracking and improve compressive, splitting tensile, and bending strengths. Guoming Liu found that polypropylene fibers (PFs) play a dominant role in enhancing the splitting tensile strength and reducing the water permeability of shotcrete [28]. Specifically, the splitting tensile strength of shotcrete with 21 mm fibers increased by 17.2% compared to shotcrete without fibers. Soner Guler found that steel (ST) fibers are significantly more effective than polyamide (PA) and fine fibrillated (FF) synthetic fibers in enhancing the strength and toughness capacities of concrete [29]. Khooshechin and Tanzadeh observed that glass fibers prevent cracking in shotcrete and effectively increase compressive, splitting tensile, and bending strengths [30]. At a 1% fiber content, splitting tensile and flexural tensile strengths increased by 12.91% and 43.38%, respectively, compared to the control group. Conversely, Baricevic et al. revealed that adding recycled tire polymer fibers (RTPFs) has a limited effect on improving the mechanical properties of shotcrete [31].

Yang et al. compared the effects of amorphous metallic fibers and steel fibers on the mechanical properties of shotcrete [32]. The results showed that amorphous metallic fibers provide higher flexural strength but exhibit lower residual strength in tension after the first crack and lower the energy absorption capability. Jeon et al. investigated the mechanical properties of polyamide fiber-reinforced shotcrete (PAFRS), focusing on toughness capacity, compressive strength, and flexural strength [33]. Their study showed that increasing the PA fiber ratio from 0.5% to 1.5% resulted in linear increases in compressive strength, direct tensile strength, bending strength, and toughness capacity. With a 1.5% fiber content, the compressive and bending strengths and toughness capacity increased by 12% and 38% compared to the control group, with the toughness capacity exceeding 11 times that of the reference group. Yan et al. investigated the effects of steel (ST) fibers and silica fume on the mechanical properties of shotcrete [34]. The results show that steel fiber-reinforced siliceous shotcrete improves the splitting tensile, flexural, and shear capacities, with maximum growth rates of 77.42%, 72.73%, and 98.31%, respectively. Steel fibers play a major role, while silica fume acts as a supplementary component. The optimal shotcrete flexural toughness was achieved when the silica fume content was 10% and the steel fiber content was 60 kg/m^3. Jeng et al. studied the effect of steel fibers on the flexural toughness of shotcrete, indicating that both the fiber ratio and aspect ratios are critical parameters for increasing the toughness capacity of shotcrete mixes [35].

Although steel fibers can effectively improve the strength and toughness of shotcrete, their heavy weight makes them difficult to disperse, and they are prone to rusting in corrosive environments. Polypropylene (PP) fibers have a low modulus of elasticity, resulting in limited improvement in shotcrete performance. Additionally, fibers like glass and basalt fibers exhibit high brittleness, which restricts their use for further applications. Polyvinyl alcohol (PVA) fibers have recently gained attention due to their high strength, elasticity modulus, acid and alkali resistance, and cost-effectiveness. When added to cement-based materials, PVA fibers significantly enhance properties such as tensile strength, crack resistance [36], impact toughness, and durability [37]. They also improve high-temperature resistance and corrosion resistance, making them a focus of engineering research. Studies on sprayed PVA-engineered cementitious composites (PVA-ECCs) [38–40] demonstrate that PVA fibers markedly improve tensile strength and deformation properties [41,42]. However, there is limited research on the effects of PVA fibers on the mechanical properties of high-performance shotcrete (HPS) and the underlying mechanisms. In addition, the durability of shotcrete is very important during its service life under different environmental conditions.

The composition design and forming method of shotcrete are significantly different from ordinary concrete [43], and shotcrete applied using pumping transportation and the jet-forming method often traps compressed air during the spraying process [44], resulting in air holes [11,45] that differentiate its pore structure from that of ordinary concrete [43,46]. Additionally, due to the low water–cement ratio in HPS, increased wind pressure is often used during spraying to meet performance requirements. The bubbles formed during this process can significantly affect the properties of HPS and should not be overlooked [47].

This study aims to fill this gap by quantitatively analyzing the influence mechanism of PVA fibers on the mechanical and durability properties of HPS. In mechanical experiments, the effects of PVA fiber on the mechanical and microstructural properties of HPS were analyzed by examining the compressive and splitting tensile strength, uniaxial compression tests, mercury intrusion porosimetry (MIP), scanning electron microscopy (SEM) tests, and bubble characteristic parameter tests to propose a practical mathematical model for the PVA-HPS uniaxial compressive stress–strain curve and establish development formulas for HPS compressive and splitting tensile strength based on PVA fiber content and age, exploring the effects of PVA fibers on the microstructure of HPS. In durability experiments, freeze–thaw cycle, electric flux, and carbonation depth tests were conducted to comprehensively analyze the frost resistance, chloride ion penetration resistance, and carbonation properties of HPS with different PVA fiber contents, analyzing the influence regularity and mechanism of

PVA fiber content on the durability of shotcrete and providing valuable insights regarding their engineering applications.

2. Materials and Methods

2.1. Raw Materials and Mixed Proportion

The main raw materials used in shotcrete include cement, silica fume, PVA fiber, coarse aggregate, fine aggregate, high-performance water reducer, and water. The cement used is P·O 42.5 Ordinary Portland Cement. The silica fume has an average particle size of 0.15 μm, a density of 2.214 g/cm^3, and a SiO2 content of at least 92%. The performance indices of the PVA fiber are detailed in Table 1, with fiber content levels at 0%, 0.25%, 0.5%, and 1%. The fine aggregate is river sand with a fineness modulus of 3.01, a bulk density of 2630 kg/m^3, and a mud content of 0.2%. The coarse aggregate is single-grade limestone crushed stone with a size range of 5 to 10 mm, a bulk density of 2820 kg/m^3, and a needle flake content of 3.7%. A polycarboxylate superplasticizer is selected for its water-reducing capabilities, with a water reduction rate of 30% and a solid content of 35%. The mix ratio is presented in Table 2.

Table 1. Performance specification of polyvinyl alcohol fiber.

Length (mm)	Diameter (mm)	Tensile Strength (MPa)	Elongation (%)	Elastic Modulus (Gpa)	Density (g.cm^{-3})
12	0.04	1560	6.5	41	1.3

Table 2. Mix proportion of shotcrete (kg/m^3).

No.	Cement	River Sand	Stone	Silica Fume	PVA Fiber	Water	Water-Reducing Agent
HPS	459	814	814	81	0	205.2	5.03
PVA-0.25%	459	810	810	81	3.3	205.2	5.03
PVA-0.50%	459	807	807	81	6.6	205.2	5.03
PVA-1.0%	459	800	800	81	13.2	205.2	5.03

PVA-0.25% means that the volume content of polyvinyl alcohol fiber is 0.25%, and the rest is analogized.

2.2. Experimental Method

2.2.1. Specimen Preparation

The shotcrete is applied using the wet spraying method. In accordance with the requirements for test specimen production outlined in the JGJ/T 372-2016 technical specifications for the application of shotcrete [48], the mold size is 450 mm × 450 mm × 120 mm. After spraying, the large panel test specimen is cured with a film, left at room temperature for one day, and then removed from the mold. Following demolding, an infrared bridge-cutting machine is used to cut the specimen. The cut specimens are then placed in a standard curing room (20 °C ± 2 °C and RH > 95%) to be cured until they reach the specified age for testing [49,50]. The complete research methodology and experimental procedure as shown in Figure 1.

In this experiment, the effects of PVA fiber on the mechanical and microstructural properties of HPS were analyzed by examining the compressive and splitting tensile strength, uniaxial compression tests, mercury intrusion porosimetry (MIP), scanning electron microscopy (SEM) tests, and bubble characteristic parameter tests; freeze–thaw cycle, electric flux, and carbonation depth tests were conducted to analyze the frost resistance, chloride ion penetration resistance, and carbonation properties of HPS with different PVA fiber contents [51]. Table 3 shows the grouping of the test, including the size and number of each test and specimen.

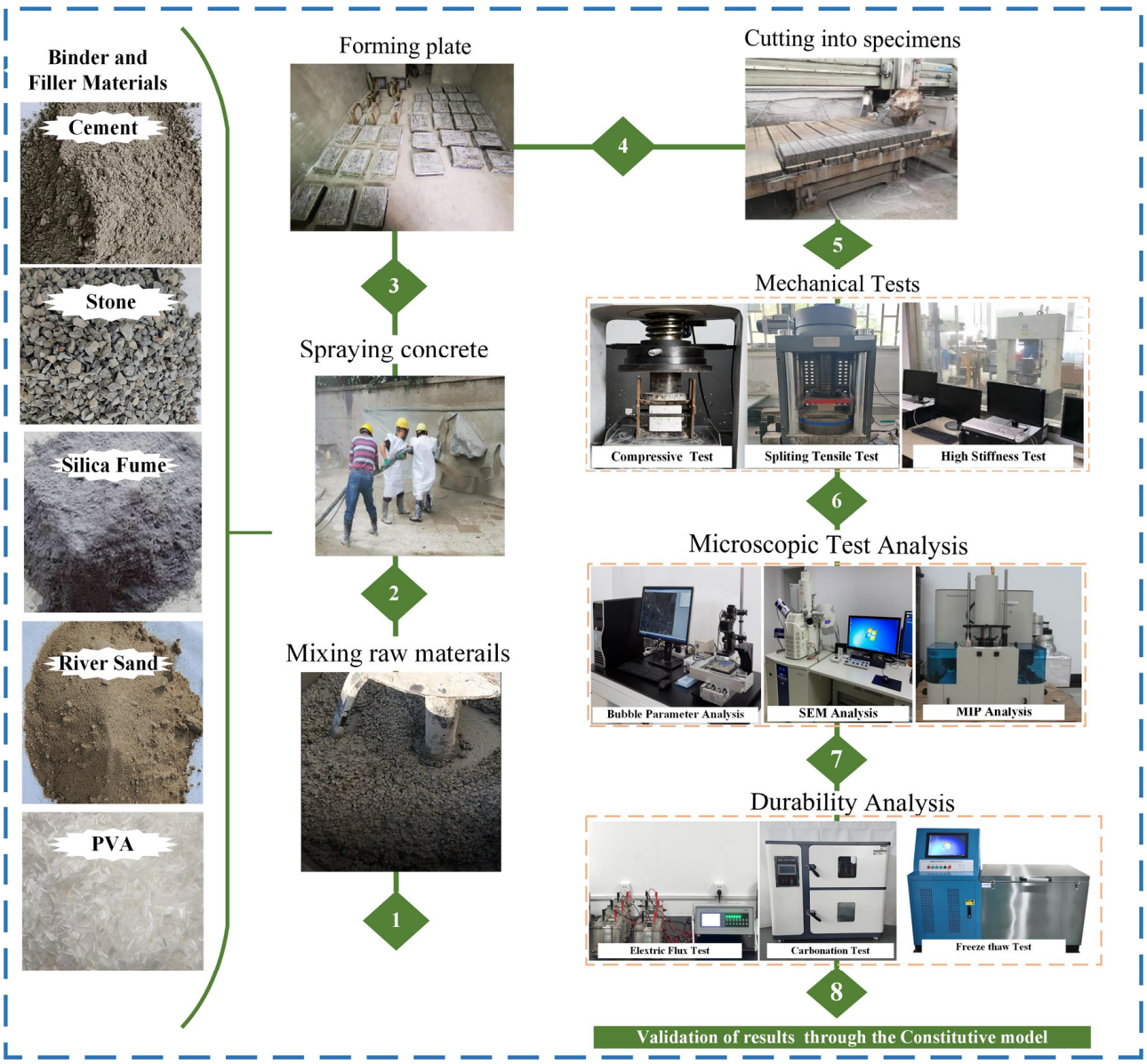

Figure 1. Complete research methodology and experimental procedure.

Table 3. Grouping of the mechanical, microstructural, and durability property tests.

Properties	Performance Index	Specimen Size	Quantity
Mechanical and microstructural properties	compressive strength	100 mm × 100 mm × 100 mm	36
	splitting tensile strength	100 mm × 100 mm × 100 mm	36
	elastic modulus	100 mm × 100 mm × 300 mm	16
	uniaxial compression test	100 mm × 100 mm × 300 mm	16
	porosity scanning electron microscopy	40 mm × 40 mm× 40 mm	12
	bubble characteristic parameter test	100 mm × 100 mm × 20 mm	12
Frost resistance	compressive strength splitting tensile strength	100 mm × 100 mm × 100 mm	168
	dynamic elastic modulus mass loss rate	100 mm × 100 mm × 400 mm	12
Chloride ion penetration resistance	electrical flux	R100 mm × 50 mm	12
Carbonation properties	carbonation depth	100 mm × 100 mm × 100 mm	48

2.2.2. Compressive and Splitting Tensile Strength Test

Shotcrete compressive strength and splitting tensile strength tests are conducted using 100 mm × 100 mm × 100 mm cubic specimens, following the requirements outlined in GB/T 50081-2019, "Standard for Test Methods of Physical and Mechanical Properties of Concrete" [52].

2.2.3. Uniaxial Compression Constitutive Test

The constitutive relationship test of shotcrete was conducted using 100 mm × 100 mm × 300 mm prismatic specimens. The loading equipment used was the material nature and damage-mechanism testing machine from Tongji University, which operates under multiple environments, as shown in Figure 2. This machine has a maximum test force of 3000 kN, and the entire test process is controlled by displacement, with a minimum displacement control accuracy of 0.06 mm/s [53].

(**a**) (**b**) (**c**)

Figure 2. Shotcrete constitutive relation experimental under uniaxial compression: (**a**) operation and data acquisition system; (**b**) experimental process; (**c**) load-destroying.

During loading, it is crucial to set an anti-friction layer between the prism specimen and the loading end to mitigate the influence of the Poisson effect on the specimen's stress state. A polytetrafluoroethylene (PTFE) plate was cut to a size of 100 mm × 100 mm, and grease was applied to the PTFE plate to serve as the friction-reducing cushion. An epsilon double-pod extensometer was used to measure the compression strain of the specimen with a measurement gauge distance of 100 mm. To reduce the influence of end looseness and unevenness on the test results, the test pieces were preloaded before formal loading. During the test, load and strain data were collected using a Nipxle-1078 data collector (National Instruments, Austin, TX, USA).

2.2.4. Bubble Characteristic Parameter Test

The bubble characteristic parameters of hardened concrete were measured using a bubble parameter tester, as shown in Figure 3a. The test was conducted in accordance with ASTM C457 [54]. Three 100 mm cube specimens were taken from each group and cut into 20 mm thick slices. The cutting surface parallel to the jet direction was used as the observation surface. The cut specimens were then ground and polished. After the test surface was dried, the pores were filled with limestone powder, using flatbed scanner scan the test surface and obtain the test surface image file, as shown by the blue areas in Figure 3b.

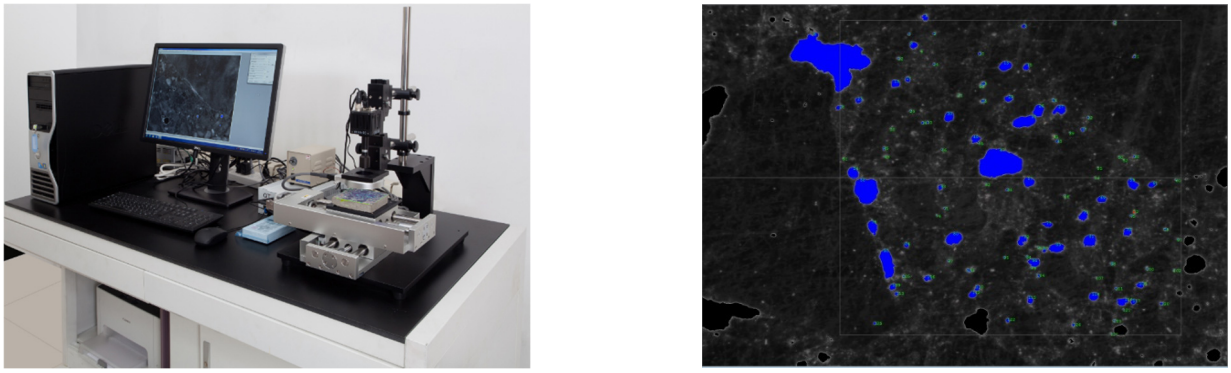

(**a**) (**b**)

Figure 3. Bubble characterization parameter testing for (**a**) hardened concrete pore structure testing; (**b**) image of the air bubbles in hardened concrete.

2.2.5. Scanning Electron Microscopy Test

Samples of HPS, PVA-0.50%, and PVA-1.0% cured for 28 days were soaked in acetone for 7 days to stop hydration. They were then dried in a vacuum-drying oven and coated with gold. The microstructure of the matrix was observed using a Quanta FEG 250 field emission environmental scanning electron microscope(FEI Ltd., Hillsboro, OR, USA).

2.2.6. Porosity Test

The porosity and pore size distribution of the HPS were analyzed using the mercury intrusion method. Samples of HPS, PVA-0.50%, and PVA-1.0% cured for 28 days were soaked in acetone for 7 days to stop hydration. The porosity was measured using an automatic mercury porosimeter with an aperture measurement range of 6 nm to 360,000 nm [55,56].

2.2.7. Durability Test

The durability performance tests include freeze–thaw resistance, chloride ion permeability, and carbonation tests. The evaluation of freeze–thaw resistance employs two types of specimens: ① 100 mm × 100 mm × 400 mm, used to determine the dynamic elastic modulus and mass loss rate after freeze–thaw cycles; ② 100 mm × 100 mm × 100 mm, used to assess compressive strength and splitting tensile strength after freeze–thaw cycles. The freeze–thaw resistance test is conducted using the rapid freezing method outlined in the standard GB/T 50082—2024 [57]. A total of 300 freeze–thaw cycles are performed. The mass loss rate and dynamic elastic modulus of the specimens are measured after every 25 cycles, while compressive strength and splitting tensile strength are assessed after every 50 cycles. The chloride ion permeability is measured using the electric flux method specified in the standard GB/T 50082—2024, with three cylindrical specimens of 100 mm × 50 mm being taken for each group. The carbonation test is conducted according to the rapid carbonation method outlined in GB/T 50082-2024. Three 100 mm cubic specimens are taken for each group. Before the test, the specimens are dried at 60 °C for 48 h. After cooling to room temperature, the surface parallel to the spraying direction is used as the test surface, while the remaining surfaces are sealed with epoxy resin. The tests are conducted at four different curing ages: 3 days, 7 days, 14 days, and 28 days. At each specified age, the carbonation depths of the specimens are measured.

3. Experiment Results and Analysis

3.1. Compressive and Splitting Tensile Strength

Figure 4 shows the effect of PVA fiber admixture on the strength of shotcrete. From Figure 4, it can be observed that, at the same age, the compressive strength of high-performance shotcrete (HPS) with PVA fibers is lower than that of HPS without fibers. The compressive strength of specimens without fibers at 1 day, 3 days, and 28 days were

36.4 MPa, 48 MPa, and 71.2 MPa, respectively. In contrast, the compressive strengths of HPS with PVA-0.25%, PVA-0.50%, and PVA-1.0% at 1 day were 15.11%, 10.44%, and 14.56% lower, respectively. As the age increased, the growth rate of compressive strength for HPS with PVA fibers was slightly lower than for HPS without fibers. After 28 days, the compressive strengths of PVA-0.25%, PVA-0.50%, and PVA-1.0% were 58.7 MPa, 60.1 MPa, and 56.8 MPa, which were 17.56%, 15.59%, and 20.22% lower than HPS without fibers, respectively.

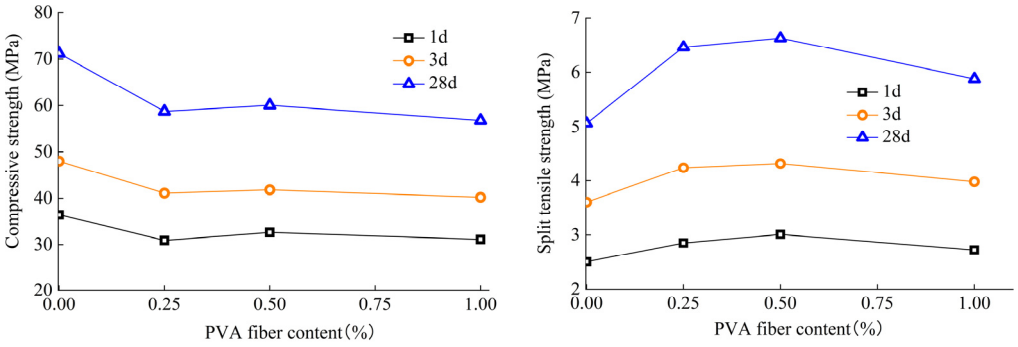

Figure 4. Effect of PVA fiber content on shotcrete strength for (**a**) compressive strength, and (**b**) splitting tensile strength.

The difference in compressive strength between different PVA fiber dosages was not significant. This reduction is attributed to the lower density of PVA fibers, which means a larger number of fibers are distributed in the same volume. This hinders even the dispersion of fibers within the concrete, leading to an increase in internal pores. During the spraying process, the randomly distributed PVA fibers tend to overlap and form a "network structure", making it easier for the matrix's internal voids to fill with large bubbles, reducing the compactness of the shotcrete's internal structure [58].

Overall, the incorporation of PVA fibers can result in a reduction in the compressive strength of high-performance shotcrete (HPS). This reduction may be due to the dense internal structure of HPS, where the addition of PVA fibers facilitates the filling of voids between particles with air bubbles, thus decreasing the matrix density. When subjected to compression, these air bubbles can lead to stress concentrations, altering the crack propagation behavior and resulting in a compressive strength lower than the reference group that did not contain fibers.

As shown in Figure 4, the splitting tensile strength of specimens without fibers at 1 day, 3 days, and 28 days were 2.50 MPa, 3.67 MPa, and 5.07 MPa, respectively. Unlike the compressive strength, the addition of PVA fibers significantly improves the splitting tensile strength of shotcrete. With increasing PVA fiber content, the splitting tensile strength of HPS initially increases and then decreases at different ages. At a PVA fiber dosage of 0.5%, the splitting tensile strengths at 1 day, 3 days, and 28 days were 3.01 MPa, 4.32 MPa, and 6.63 MPa, which were 20.40%, 19.67%, and 30.77% higher than HPS without fiber, respectively. When the PVA fiber content increased to 1.0%, the splitting tensile strength of HPS decreased, but it remained higher than that of HPS without fibers.

The tensile-to-compressive strength ratio can reflect the toughness of shotcrete. Figure 5 shows the effect of PVA fiber content on the shotcrete tensile-to-compression ratio. From Figure 5, it can be seen that, as the amount of PVA fibers increases, the tensile-to-compressive ratio of the HPS initially rises and then falls. Overall, the tensile-to-compressive ratio of HPS incorporating PVA fibers is significantly higher than HPS without fibers, and this ratio gradually increases with age. When the PVA fiber content reaches 0.5%, the tensile-to-compressive ratio of HPS reaches the maximum value, which is more than 30% higher than that of HPS without fibers.

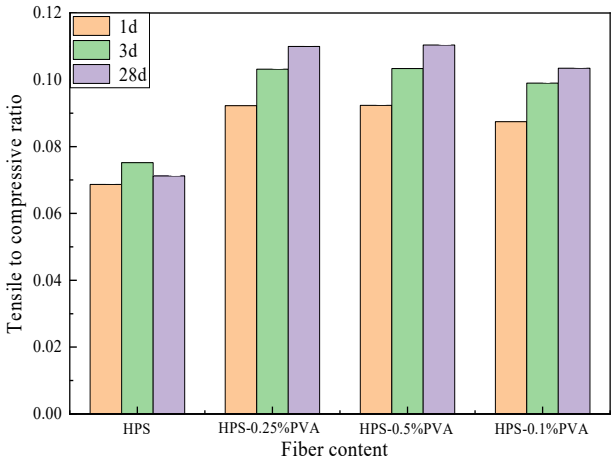

Figure 5. Effect of PVA fiber content on HPS tensile-to-compression ratio.

The relationship between the fiber types and dosages in regard to the strength of shotcrete in the literature was analyzed in this study, as illustrated in Figure 6. As shown in the figure, the compressive strength of shotcrete in existing studies is mostly concentrated at C50 or below. Under the same dosage, steel fibers exhibit a more significant improvement in the compressive strength of shotcrete compared to other fibers. In terms of tensile strength, the incorporation of fibers into shotcrete can effectively enhance its tensile strength. Comparatively, carbon fibers, steel fibers, and PVA fibers exhibit the most significant levels of improvement. Moreover, there appears to be an optimal fiber dosage for enhancing tensile strength which typically ranges between 0.50% and 1.0%. Since shotcrete is produced using a specialized forming process, the physical and chemical properties of the raw materials, accelerators, water reducers, and other admixtures, as well as the flowability and cohesiveness of the mixture during pumping and the fiber–matrix gradation, all have a significant impact on the strength of shotcrete. Therefore, these factors need to be systematically considered.

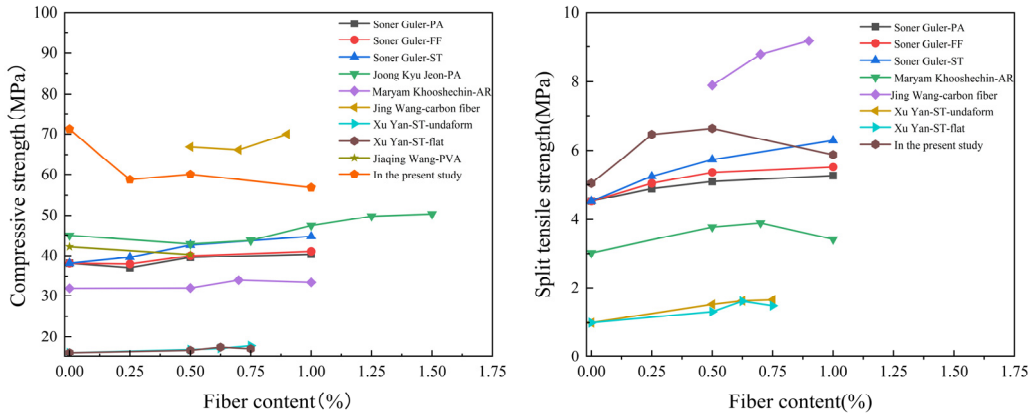

(**a**) (**b**)

Figure 6. The effect of fiber types and dosage on the strength of shotcrete [14,26,29,30,33,34]. (**a**) compressive strength, (**b**) splitting tensile strength.

Based on the above analysis, it is evident that the compressive strength and splitting tensile strength of shotcrete with PVA fibers are influenced by both the PVA fiber content and the age of the shotcrete. The analysis reveals that these strengths follow a logarithmic relationship with age, as illustrated in Figure 7, $f_{cc}(t) = k_{cc} \cdot \ln(t)$; $f_{ts}(t) = k_{ts} \cdot \ln(t)$. The parameters k_{cc} and k_{ts} for shotcrete with various mix proportions are detailed in Table 4.

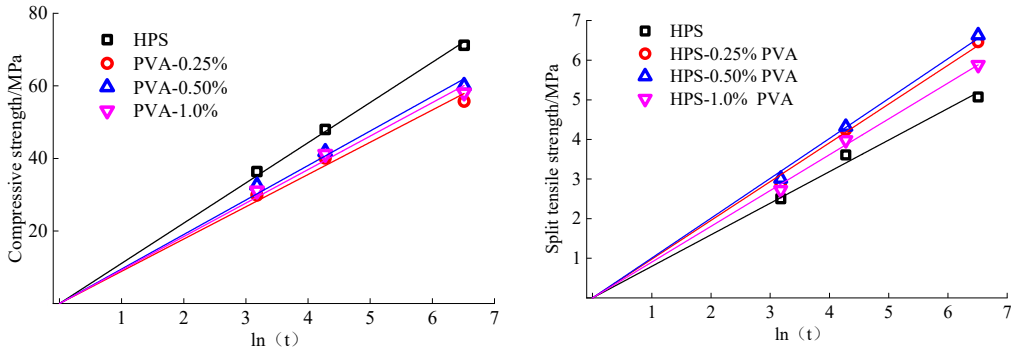

(**a**) (**b**)

Figure 7. The relationship curve between HPS strength development and age, with different PVA fiber contents for (**a**) $f_{cc}(t)$-ln(t), and (**b**) $f_{ts}(t)$-ln(t).

Table 4. Different PVA fiber content k_{cc} and k_{ts}.

	HPS	PVA-0.25(%)	PVA-0.50(%)	PVA-1.0(%)
k_{cc}	11.085	9.393	9.514	9.232
R^2	0.999	0.997	0.998	0.998
k_{ts}	0.797	0.978	1.006	0.904
R^2	0.998	0.998	0.999	0.999

Figure 8a,b show the effects of PVA fibers on k_{cc} and k_{ts}, respectively, and the effects of PVA fibers on k_{cc} and k_{ts} can be expressed by Equations (1) and (2).

$$k_{cc} = 9.171 + 1.913.\exp^{(-3.441PVA)} \quad (1)$$

$$k_{ts} = 0.805 + 0.775PVA - 0.679(PVA)^2 \quad (2)$$

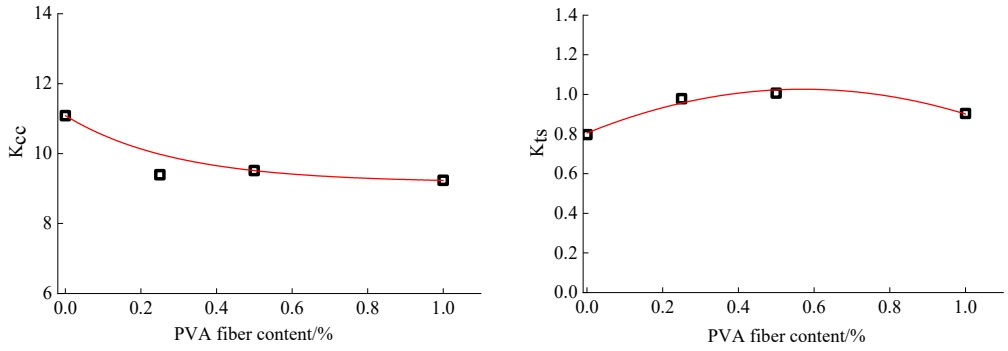

(**a**) (**b**)

Figure 8. Effect of PVA fiber content on k_{cc} and k_{ts} value for (**a**) PVA-K_{cc}, and (**b**) PVA-K_{ts}.

Finally, the development formula of compressive strength and the splitting tensile strength of HPS based on PVA fiber content and age is obtained; these formulas are presented in Equations (3) and (4).

$$f_{cc}(t) = \left(9.171 + 1.913.\exp^{(-3.441PVA)}\right) \cdot \ln(t) \quad (3)$$

$$f_{ts}(t) = \left(0.805 + 0.775\ PVA - 0.679(PVA)^2\right) \cdot \ln(t) \quad (4)$$

Here, PVA denotes the polyvinyl alcohol volume fraction (%), f_{cc} represents the cubic compressive strength of the concrete (MPa), f_{ts} indicates the splitting tensile strength of the concrete (MPa), and t is the age of the concrete (h).

3.2. Uniaxial Compressive Constitutive Relationship

3.2.1. Uniaxial Compression Stress–Strain Curve

The compressive stress–strain curves for different PVA fiber contents are illustrated in Figure 9. The average values of the uniaxial compressive stress–strain curves are summarized in Table 5. As observed from the table, the peak stress and elastic modulus of high-performance shotcrete (HPS) without PVA fibers are higher than those of HPS containing PVA fibers. Specifically, with an increasing PVA fiber content, the peak stress of HPS initially decreases and then rises, while the elastic modulus shows a consistent decline. Compared to HPS, the peak stress of HPS with PVA-0.25%, PVA-0.50%, and PVA-1.0% decreased by 21.35%, 17.93%, and 10.99%, respectively, and the elastic modulus decreased by 8.09%, 9.70%, and 12.67%, respectively.

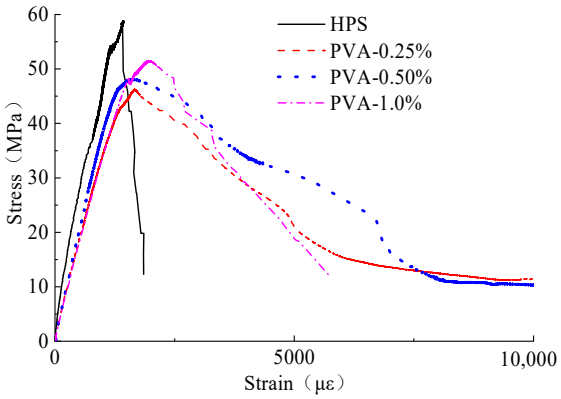

Figure 9. Compressive stress–strain curve of shotcrete with different mix proportions.

Table 5. Average characteristic value of a stress–strain curve under uniaxial compression.

No.	Peak Stress (MPa)	Peak Strain (με)	Elastic Modulus (GPa)
HPS	58.78	1433.17	37.1
PVA-0.25%	46.23	1671.20	34.1
PVA-0.50%	48.24	1617.84	33.5
PVA-1.0%	52.32	1884.77	32.4

Despite the reduction in peak stress and elastic modulus due to the inclusion of PVA fibers, the peak strain of HPS increases with a higher fiber content. Specifically, the peak strain of HPS with PVA-0.25%, PVA-0.50%, and PVA-1.0% increased by 16.61%, 12.89%, and 31.51%, respectively, compared to HPS without fibers.

The stress–strain curves of HPS incorporating PVA fibers exhibit a more gradual ascent and a slower decline after reaching the peak stress compared to HPS without fibers.

In the process of compression, multiple cracks were observed in the PVA fiber-reinforced shotcrete. The inclusion of fibers helped in distributing the stress more evenly across the matrix, which led to the formation of multiple smaller cracks rather than a single large crack. This behavior aligns with the typical crack-bridging effect of fibers, and this suggests a transition from brittle to ductile failure, which enhances the ductility and toughness of the shotcrete. Although the peak stress is reduced with PVA fibers, the increased peak strain indicates enhanced deformation resistance. Additionally, the post-peak curve shows a larger area enclosed by the coordinate axes, highlighting improved energy dissipation. This behavior underscores the toughening effect of PVA fibers, which effectively suppress microcrack formation and enhance the descending section of the stress–

strain curve, thereby improving the material's overall deformation resistance and energy absorption capacity.

3.2.2. Uniaxial Compression Constitutive Equation

The obtained compression stress–strain curves of shotcrete with different mix proportions are averaged and normalized as dimensionless, as shown in Equations (5) and (6). This normalization allows for a clearer comparison of the effects of different PVA fiber contents on the stress–strain behavior of the shotcrete. The normalization process involves scaling the stress and strain values to a dimensionless format to facilitate direct comparisons between the different mix proportions.

$$x = \varepsilon / \varepsilon_0 \tag{5}$$

$$y = \sigma / f_c \tag{6}$$

where, ε_0 is the peak strain and f_c is the axial compressive strength, which is the peak stress. Based on the test results from this study, and through referencing the relevant literature, the classical concrete stress–strain curve equation has been adopted. The equation is formulated as follows in Equations (7) and (8):

$$y = ax + (3 - 2a)x^2 + (a - 2)x^3 \quad x \leq 1 \tag{7}$$

$$y = \frac{x}{b(x-1)^2 + x} \quad x \geq 1 \tag{8}$$

The constitutive relationship curves and the full curve equation for High-Performance Shotcrete (HPS) incorporating polyvinyl alcohol (PVA) fibers are compared in Figure 10. The parameters of the constitutive equations, as determined from the fitting process, are listed in Table 6. From the table, it is evident that the overall fitting performance of the constitutive equations is satisfactory, accurately representing the stress–strain behavior of HPS with different PVA fiber contents. This demonstrates that the adopted model effectively captures the mechanical properties and response characteristics of the HPS samples under various conditions.

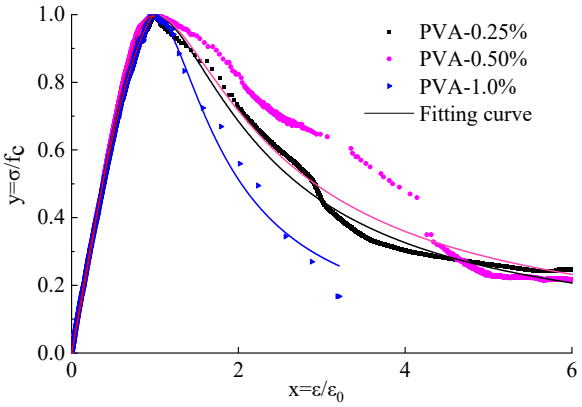

Figure 10. Compressive stress–strain and equation fitting curve of shotcrete (dimensionless).

Table 6. Shotcrete constitutive model parameters under uniaxial compression.

No.	Ascend Parameter a	R^2	Descend Parameter b	R^2
HPS	1.312	0.999	36.073	0.97
PVA-0.25%	1.326	0.999	0.919	0.98
PVA-0.50%	1.210	0.999	0.793	0.94
PVA-1.0%	1.434	0.999	9.772	0.99

3.3. Microstructure Analysis

3.3.1. Pore Structure

The PVA-HPS under different PVA fiber contents at an age of 28 d was selected for MIP experiments. According to the results of the mercury injection test, the pore size is divided into three intervals: 3 nm–50 nm, 50–1000 nm, >1000 nm. The relationship between dV/dlogD and the pore size of PVA-HPS under different fiber contents is shown in Figure 11a. The pore volume of PVA-HPS under different fiber contents is shown in Figure 11.

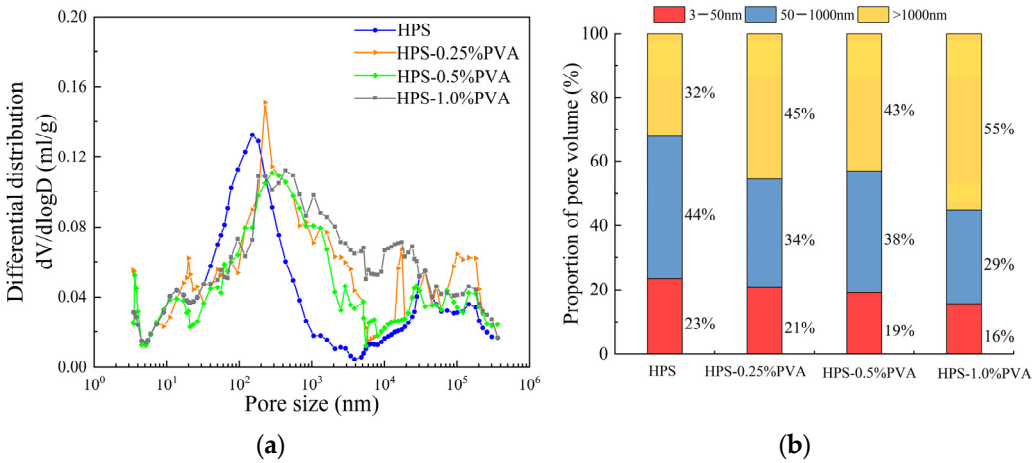

Figure 11. Comparative study of pore characteristics of PVA-HPS under different fiber contents. (**a**) The relationship between dV/dlogD and pore size; (**b**) Proportion of pore volume.

From the analysis of the figure, it can be concluded that, as the amount of PVA fiber increases, the most probable pore size gradually enlarges, while the proportion of gel pores smaller than 50 nm decreases. When the fiber content reaches 1.0%, the proportion of gel pores drops from 22.72% to 15.23%, whereas the proportion of large pores over 1000 nm increases significantly from 31.25% to 52.96%. This suggests that incorporating PVA increases the proportion of pores larger than 50 nm, particularly large pores, leading to a coarser pore structure. When the fiber content exceeds 0.50%, the increase in large pores becomes more pronounced.

3.3.2. Matrix Microstructure

Figure 12 shows the microstructure of shotcrete with different mix proportions. It can be seen from Figure 12a that the HPS matrix has a dense structure, likely attributed to the low water-to-binder ratio and high matrix strength of HPS. Additionally, the inclusion of silica fume enhances the compactness of the matrix.

Figure 12b shows that PVA fibers integrate well with the matrix, penetrating and bonding closely. During stress application, these fibers bridge across cracks, effectively transferring stress and reducing stress concentrations at the crack tips. This bridging effect helps form an adhesive structure at both ends of the crack, while the three-dimensional network of overlapping PVA fibers in the matrix helps to inhibit crack propagation. This explains the observed improvements in splitting tensile strength and peak strain in HPS with PVA fibers [59]. However, as shown in Figure 12c, a higher dosage of PVA fibers can lead to uneven distribution within the specimen, creating weak interfaces between the fibers and matrix. This can adversely affect tensile properties. Therefore, while PVA fibers can enhance the toughness and crack resistance of shotcrete, it is crucial to select an optimal fiber dosage to maximize these benefits and improve the overall tensile strength of high-performance shotcrete.

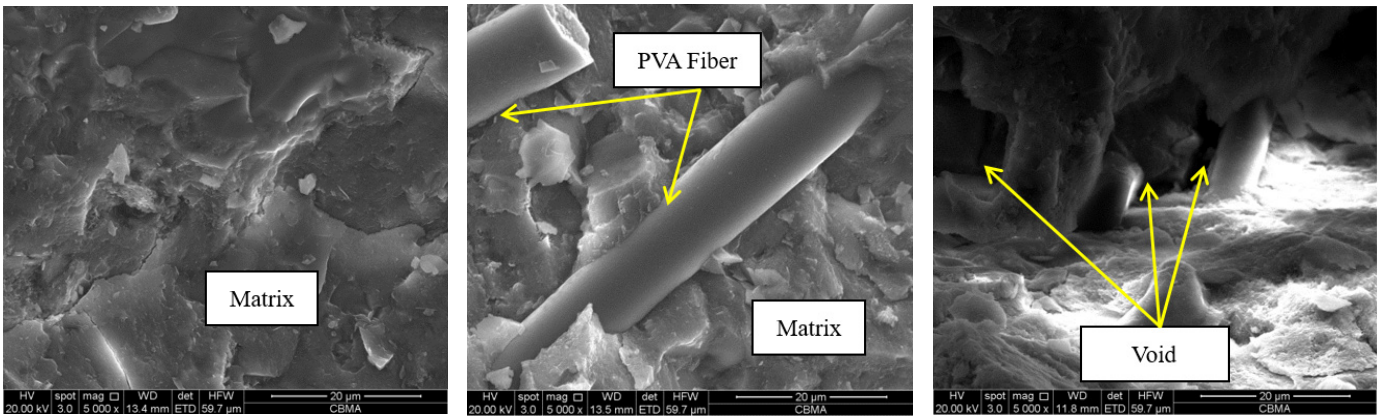

(**a**) (**b**) (**c**)

Figure 12. Microstructure of shotcrete with different mix proportions: (**a**) HPS; (**b**) PVA-0.50%; (**c**) PVA-1.0%.

3.3.3. Bubble Characteristic Parameters

Figure 13 presents the changes in bubble characteristics of HPS with varying PVA fiber contents. In Figure 13a, it can be observed that, as the PVA fiber content increases, the number of bubbles in HPS gradually decreases while the volume content of the bubbles increases. Notably, when the fiber content exceeds 0.5%, there is a sharp increase in the bubble volume content. Specifically, for PVA-1.0%, the number of bubbles is reduced by 16.56% compared to HPS but the bubble volume content increases by 24.15%. This indicates a significant increase in bubble size with the addition of PVA fibers.

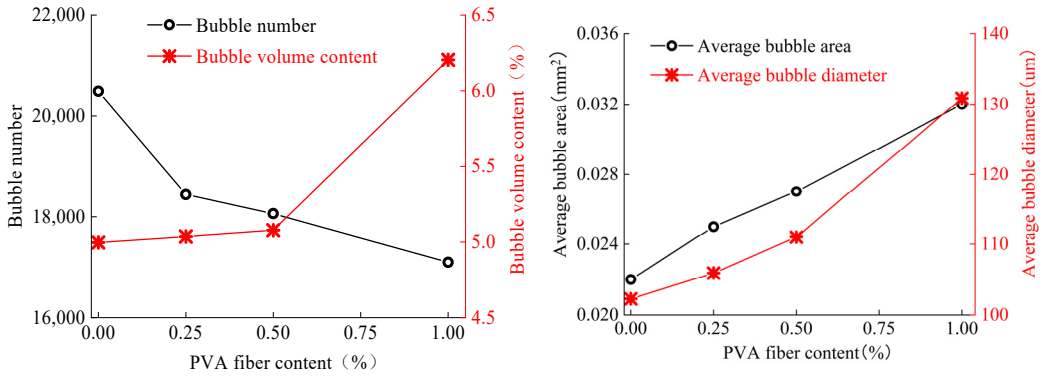

(**a**) (**b**)

Figure 13. The variation curve of shotcrete bubble characteristic parameters under different PVA fiber contents for (**a**) bubble number and bubble volume content and (**b**) the average bubble area and average bubble diameter.

Figure 13b shows that the average bubble area and average bubble diameter of HPS both increase significantly with a higher fiber content. The average bubble area for PVA-0.25%, PVA-0.50%, and PVA-1.0% increased by 13.64%, 22.73%, and 45.45%, respectively, while the average bubble diameter increased by 3.56%, 8.53%, and 27.95%.

The growth rate of the average bubble area is higher than that of the average bubble diameter, indicating that the bubbles become more irregular with increased PVA fiber content. This effect is attributed to the lower density of PVA fibers, which leads to a higher concentration of fibers per unit volume. During the spraying process, the numerous randomly oriented PVA fibers create obstacles to the expulsion of air, resulting in a higher volume content and larger-sized bubbles in HPS.

Figure 14 illustrates the pore volume distribution of HPS with varying PVA fiber contents, categorized into four size ranges: 0–200 μm, 200–500 μm, 500–1200 μm, and

>1200 μm. The figure reveals that HPS with different PVA fiber contents shows a higher pore volume ratio in the ranges of 200–500 μm, 500–1200 μm, and >1200 μm compared to HPS without fibers.

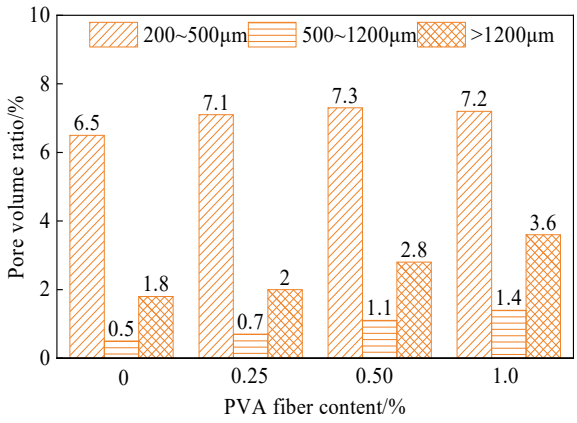

Figure 14. Bubble pore volume distribution of HPS under different PVA fiber contents.

Specifically, the pore volume ratios for PVA-0.25%, PVA-0.50%, and PVA-1.0% in the 0–200 μm range decreased by 1.10%, 2.63%, and 3.73%, respectively, relative to HPS. Conversely, the pore volume ratios in the 200–500 μm range increased by 9.23%, 12.31%, and 10.77%, respectively. Notably, the ratios in the 500–1200 μm range increased by 11.11%, 55.56%, and 100% for PVA-0.25%, PVA-0.50%, and PVA-1.0%, respectively. Additionally, for pores larger than 1200 μm, the volume ratios increased by 40%, 120%, and 180% for PVA-0.25%, PVA-0.50%, and PVA-1.0%, respectively.

The increased volume ratios of larger pores (500–1200 μm and >1200 μm) with a higher PVA fiber content indicates a reduction in the compactness of the HPS matrix. This reduced density of the matrix is likely detrimental to the development of compressive strength, potentially explaining why the addition of PVA fibers results in decreased compressive strength and peak stress under uniaxial compression [60]. The larger and more numerous voids created by the PVA fibers negatively impact the overall structural integrity of the HPS.

4. Influence of the PVA Fiber on the Durability of High-Performance Shotcrete

4.1. Freeze–Thaw Cycle Test

4.1.1. Mass Loss Rate and Relative Dynamic Elastic Modulus

Figure 15a shows the variation curve of the mass loss rate of PVA-HPS under freeze–thaw cycles. As shown in the figure, the mass loss rate variation curves of different PVA-HPS mix proportions exhibit a two-stage pattern, with 225 freeze–thaw cycles as the turning point. Within the range of 0 to 225 cycles, the mass loss rate increases slowly. After 225 freeze–thaw cycles, the mass loss rates for HPS, HPS-0.25% PVA, HPS-0.50% PVA, and HPS-1.0% PVA are 0.48%, 0.23%, 0.25%, and 0.36%, respectively. This is because the continued action of freeze–thaw cycles, along with alternating temperatures and crystallization stress, leads to ongoing damage to the matrix, causing an increase in the mass loss rate. As the freeze–thaw cycles continue, the mass loss rate of all PVA-HPS mix proportions shows a decreasing trend. After 300 freeze–thaw cycles, the mass loss rates for HPS, HPS-0.25% PVA, HPS-0.50% PVA, and HPS-1.0% PVA are 0.26%, 0.09%, 0.03%, and 0.14%, respectively. This is due to the continuous action of the expansion stress generated by the hydrostatic pressure during the freeze–thaw cycle. Cracks appear inside the matrix and the external water penetrates into the bubbles inside the concrete along the cracks, resulting in an increase in the quality of the specimen [61]. The mass loss rate of PVA fiber-reinforced HPS is significantly lower than that of HPS without fibers. This is because the incorporation of PVA fibers creates larger inter-particle pores within the HPS matrix, allowing moisture to penetrate more easily into the matrix compared to HPS without fibers.

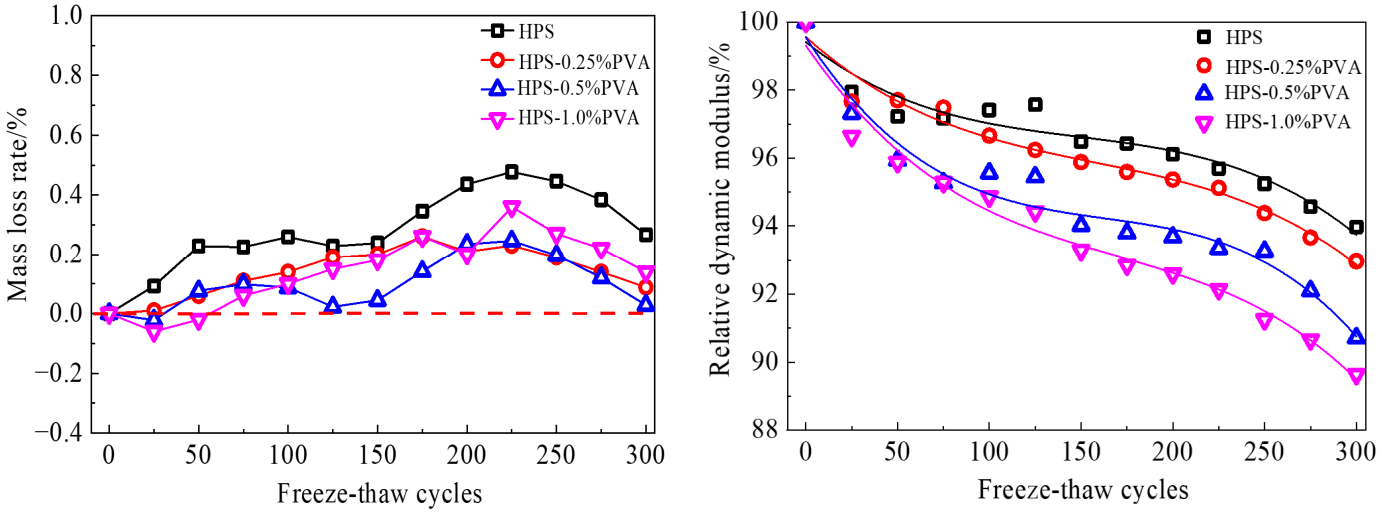

Figure 15. The impact of PVA fibers on the mass loss rate and relative dynamic elastic modulus of HPS. (**a**) Mass loss rate and (**b**) relative dynamic elastic modulus.

Figure 15b shows the variation curves of the relative dynamic elastic modulus for PVA-HPS under freeze–thaw cycles. As shown in the figure, the relative dynamic elastic modulus variation curves of different PVA-HPS mix proportions exhibit a two-stage pattern, with 200 freeze–thaw cycles as the turning point. Within a range of 0 to 200 cycles, the relative dynamic elastic modulus of all PVA-HPS mix proportions decreases slowly. After 200 freeze–thaw cycles, the relative dynamic elastic modulus of HPS, HPS-0.25% PVA, HPS-0.50% PVA, and HPS-1.0% PVA decreases by 3.89%, 4.63%, 6.32%, and 7.40%, respectively. With the continued increase in freeze–thaw cycles, the relative dynamic elastic modulus of all PVA-HPS mix proportions shows an increasing trend, which is particularly pronounced in the PVA-0.50% and PVA-1.0% groups. After 300 freeze–thaw cycles, the relative dynamic elastic modulus of HPS, HPS-0.25% PVA, HPS-0.50% PVA, and HPS-1.0% PVA decreased by 6.03%, 7.03%, 9.29%, and 10.36%, respectively. This indicates that HPS exhibits the least damage under freeze–thaw cycles. This is due to two factors: on the one hand, HPS contains 15% silica fume, which enhances the concrete's density and refines the pore structure [46]. On the other hand, the spray-forming process used for HPS exerts a compacting effect on the shotcrete, further improving the matrix's density and contributing to its strong freeze–thaw resistance. Additionally, PVA fibers have a low density and large specific surface area per unit volume, which makes them prone to agglomeration during the mixing process. This negatively affects the packing of the concrete, resulting in larger inter-particle voids within the matrix. These voids are easily filled by air bubbles, leading to a lower matrix density in PVA-reinforced HPS compared to HPS without fibers.

By performing a polynomial fitting of the relative dynamic elastic modulus Er and the number of freeze–thaw cycles n, the fitted relationship is given by Equations (9)–(12). The fitting results indicate that Er and n follow a cubic polynomial relationship.

$$\text{HPS: } E_r = 99.41 - 4.27 \times 10^{-2}n + 2.41 \times 10^{-4}n^2 - 5.40 \times 10^{-7}n^3 \quad R^2 = 0.91 \tag{9}$$

$$\text{HPS-0.25\%: } E_r = 99.56 - 4.84 \times 10^{-2}n + 2.37 \times 10^{-4}n^2 - 5.02 \times 10^{-7}n^3 \quad R^2 = 0.96 \tag{10}$$

$$\text{HPS-0.50\%: } E_r = 99.41 - 8.29 \times 10^{-2}n + 4.63 \times 10^{-4}n^2 - 9.47 \times 10^{-7}n^3 \quad R^2 = 0.95 \tag{11}$$

$$\text{HPS-1.0\%: } E_r = 999.41 - 7.85 \times 10^{-2}n + 3.71 \times 10^{-4}n^2 - 7.28 \times 10^{-7}n^3 \quad R^2 = 0.97 \tag{12}$$

Referring to the calculation method for the durability index of ordinary concrete, the durability factor (DF) is calculated as DF = PN/300, where DF is the durability index of the shotcrete, N is the number of freeze–thaw cycles at the end of the test, and P is the relative

dynamic elastic modulus at the end of the freeze–thaw test. The calculations show that the freeze–thaw durability indices of all PVA-HPS mix proportions are above 90%, indicating excellent freeze–thaw resistance, which meets the freeze–thaw performance requirements for cold regions [62].

4.1.2. Strength

The variation curve of compressive strength of HPS under freeze–thaw cycles is shown in Figure 16a, and the variation curve of compressive strength loss rate is shown in Figure 16b. As shown in the figure, with the increase in freeze–thaw cycles, the compressive strength of all PVA-HPS mix proportions shows a slow decline. After 200 freeze–thaw cycles, the compressive strength loss rates for HPS, HPS-0.25% PVA, HPS-0.50% PVA, and HPS-1.0% PVA are −10.26%, −0.18%, −4.40%, and −2.31%, respectively. The compressive strength of each group remains higher than it was before the freeze–thaw cycles. After 300 freeze–thaw cycles, the compressive strength loss rates are −4.14%, 1.77%, −1.76%, and 0.04% for HPS, HPS-0.25% PVA, HPS-0.50% PVA, and HPS-1.0% PVA, respectively. The compressive strength shows virtually no decline. This indicates that PVA-HPS exhibits excellent freeze–thaw resistance. This may be attributed to two factors, as, on the one hand, the shotcreting process compacts the concrete, further enhancing the matrix density and giving it strong inherent freeze–thaw resistance; on the other hand, the low water–binder ratio of HPS and the incorporation of 15% silica fume contribute to its durability. During freeze–thaw cycles, the water that infiltrates the matrix reacts with unhydrated cement and silica fume, leading to further hydration. The CSH gel produced from this secondary hydration makes the structure of the shotcrete matrix even more dense.

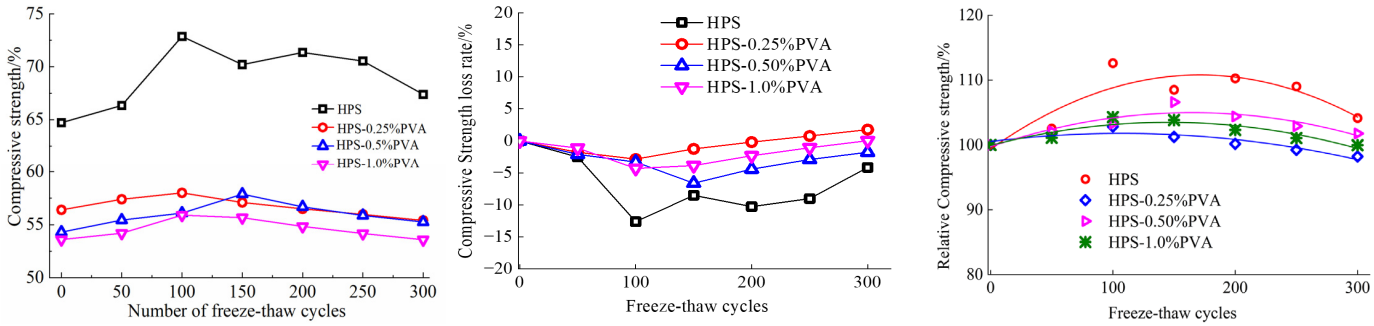

(**a**) (**b**) (**c**)

Figure 16. The variation compressive strength of PVA-HPS under freeze–thaw cycles. (**a**) Compressive strength, (**b**) compressive strength loss rate, and (**c**) relative compressive strength.

There are two main forms of freeze–thaw damage in concrete: frost heave cracking and freeze–thaw erosion. Due to the low water–binder ratio and the addition of silica fume, which further enhances the matrix density, the freeze–thaw damage in HPS during freeze–thaw cycles primarily manifests as surface spalling caused by freeze–thaw erosion rather than internal cracking. In contrast, the dynamic elastic modulus is more sensitive to surface damage in concrete. Therefore, during the freeze–thaw cycles, the decrease in the relative dynamic elastic modulus for different HPS mix proportions is greater than the reduction in compressive strength.

Figure 16c shows the variation curve of relative compressive strength. A polynomial fitting was applied to the relative compressive strength C_r and the number of freeze–thaw cycles n, and the fitting results are shown in Equations (13)–(16). The results indicate that C_r and n follow a quadratic polynomial relationship.

$$\text{HPS: } C_r = 99.38 + 0.13n - 3.90 \times 10^{-4}n^2 \quad R^2 = 0.79 \tag{13}$$

$$\text{HPS-0.25\%: } C_r = 100.54 + 0.02n - 1.09 \times 10^{-4}n^2 \quad R^2 = 0.83 \tag{14}$$

$$\text{HPS-0.50\%: } C_r = 99.73 + 0.06n - 1.94 \times 10^{-4}n^2 \quad R^2 = 0.83 \tag{15}$$

$$\text{HPS-1.0\%: } C_r = 99.93 + 0.05n - 1.68 \times 10^{-4}n^2 \quad R^2 = 0.84 \tag{16}$$

During the freeze–thaw cycles, the compressive strength of HPS is influenced by both the secondary hydration of cement and silica fume, as well as the freezing stress generated by the cycles. As a result, the compressive strength undergoes alternating changes, which occur relatively slowly. This dynamic behavior affects the correlation accuracy of the fitted polynomial equation.

The variation curve of splitting tensile strength of shotcrete under freeze–thaw cycles is shown in Figure 17a, and the variation curve of splitting tensile strength loss rate is shown in Figure 17b. As shown in the figure, with the increase in freeze–thaw cycles, the splitting tensile strength loss rate of HPS significantly increases. The splitting tensile strength loss rates of HPS with different PVA fiber contents are noticeably lower than the reference group without PVA fiber, with the PVA-0.50% mix showing the best performance. As the number of freeze–thaw cycles increases, the splitting tensile strength of HPS decreases significantly. After 200 freeze–thaw cycles, the splitting tensile strength is 3.54 MPa, with a strength loss rate of 30.2%. After 300 freeze–thaw cycles, the splitting tensile strength further decreases to 3.04 MPa, with the strength loss rate reaching 40%.

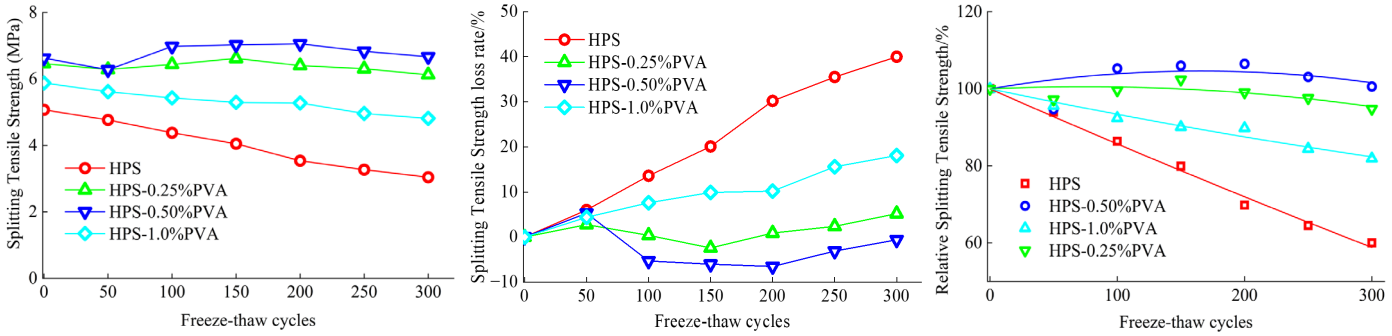

(**a**) (**b**) (**c**)

Figure 17. The variation splitting tensile strength of PVA-HPS under freeze–thaw cycles. (**a**) Splitting tensile strength; (**b**) splitting tensile strength loss rate; (**c**) relative splitting tensile strength.

Before freeze–thaw cycles, the splitting tensile strengths of HPS-0.25% PVA, HPS-0.50% PVA, and HPS-1% PVA were 6.46 MPa, 6.63 MPa, and 5.88 MPa, respectively, which represent increases of 27.44%, 30.69%, and 15.88% compared to HPS. During the freeze–thaw cycles, the splitting tensile strength loss rates of HPS-0.25% PVA, HPS-0.50% PVA, and HPS-1% PVA were significantly lower than that of HPS. After 200 freeze–thaw cycles, the splitting tensile strength loss rates for HPS-0.25% PVA, HPS-0.50% PVA, and HPS-1% PVA were 0.9%, −6.5%, and 10.2%, respectively. After 300 freeze–thaw cycles, the loss rates were 5.2%, −0.6%, and 18.1%, respectively. This demonstrates that the tensile performance of HPS-0.25% PVA, HPS-0.50% PVA, and HPS-1% PVA under freeze–thaw cycles is significantly superior to that of HPS. Among them, there is an optimal PVA fiber content, with HPS-0.50% PVA showing the best freeze–thaw resistance.

Figure 17c shows the relationship curve between the number of freeze–thaw cycles and the relative splitting tensile strength. By performing a polynomial fitting of the relative splitting tensile strength S_r and the number of freeze–thaw cycles n, the resulting relationship can be expressed through the fitted polynomial equation. The fitting results are shown in equations (17)–(20), indicating that the relationship between the relative splitting tensile strength S_r and the number of freeze–thaw cycles n follows a quadratic polynomial relationship.

$$\text{HPS: } S_r = 100 - 14.58 \times 10^{-2}n + 0.29 \times 10^{-4}n^2 \quad R^2 = 0.99 \tag{17}$$

$$\text{HPS-0.25\%PVA: } S_r = 100 + 1.53 \times 10^{-2}n - 1.02 \times 10^{-4}n^2 \quad R^2 = 0.99 \tag{18}$$

$$\text{HPS-0.50\%PVA: } S_r = 100 + 5.61 \times 10^{-2}n - 1.70 \times 10^{-4}n^2 \quad R^2 = 0.99 \tag{19}$$

$$\text{HPS-1.0\%PVA: } S_r = 100 - 6.94 \times 10^{-2}n + 0.36 \times 10^{-4}n^2 \quad R^2 = 0.99 \tag{20}$$

During the freeze–thaw cycles, the damage sustained by HPS is primarily characterized by surface spalling caused by freeze–thaw erosion. In comparison, the splitting tensile strength is more sensitive to surface damage in concrete. Therefore, during the freeze–thaw cycles, the decline in the splitting tensile strength of HPS is significantly greater than the reduction in compressive strength. The incorporation of PVA fibers inhibited the formation and development of early drying shrinkage cracks in shotcrete and increased the tortuosity of connected capillary pores [63]. During the freeze–thaw process, PVA fibers play a dual role. On the one hand, they inhibit the surface spalling of HPS, reducing freeze–thaw erosion damage. Simultaneously, PVA fibers limit the damage and destruction caused by freezing stress in the shotcrete matrix, suppressing the connection and expansion of large pore air bubbles within the matrix. On the other hand, under stress, PVA fibers can mitigate stress concentration at microcrack tips caused by crack propagation, altering the deflection direction of microcracks and enhancing the tensile performance of the matrix [64].

HPS has a low water–binder ratio, and PVA fibers have a relatively low density, resulting in a higher number of fibers per unit volume. At higher dosages, the PVA fibers become difficult to distribute evenly within the specimen, effectively increasing the number of weak fiber–matrix interfaces. This negatively impacts the tensile performance of HPS during the freeze–thaw cycle. Therefore, for HPS, a higher PVA fiber content is not always better. A reasonable selection of the PVA fiber dosage can effectively optimize the fiber's toughening and crack-inhibiting effects within the matrix.

4.1.3. Five-Dimensional Evaluation Diagram

Based on the results of the freeze–thaw cycle tests, five indicators were selected for analysis in this study: compressive strength, splitting tensile strength, tensile-to-compressive strength ratio, mass loss rate, and relative dynamic elastic modulus. These indicators were compared and analyzed using the five-dimensional evaluation method [65]. The five-dimensional evaluation chart for HPS with different PVA fiber contents is shown in Figure 18. As shown in Figure 18, when the PVA fiber content is 0.50%, HPS achieves a good balance between compressive strength and tensile strength, while the mass loss rate and relative dynamic elastic modulus also exhibit a well-balanced performance. This indicates that HPS with 0.50% PVA fiber content exhibits excellent durability in terms of resistance to frost heave cracking and freeze–thaw erosion. Additionally, from an engineering application perspective, a 0.5% PVA fiber content not only maximizes the fiber's toughening effect but also balances cost considerations, making it a practical and feasible optimization solution.

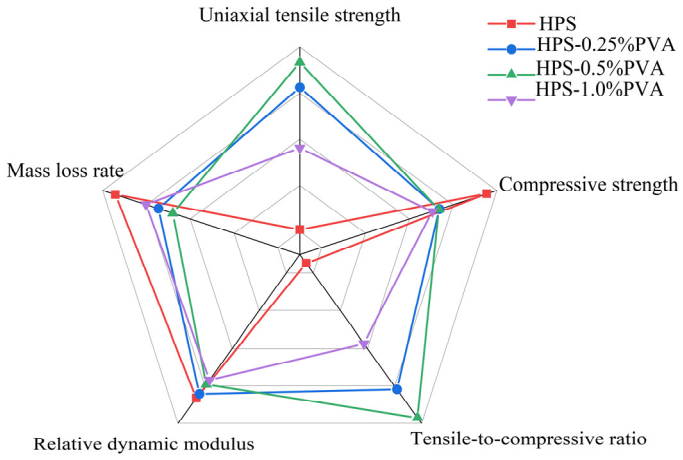

Figure 18. Five-dimensional evaluation diagram of PVA-HPS.

4.2. Electrical Flux

Chloride ion erosion is an important factor affecting the durability of concrete. The chloride ion penetration resistance of high-performance concrete (HPS) was compared using electrical flux, and the effect of PVA fiber content on the electrical flux of HPS was also studied. Figure 19 shows the effect of PVA fiber content on the electrical flux of HPS. As shown in the figure, the electrical flux of all HPS mixtures was relatively low, indicating excellent chloride ion permeability resistance.

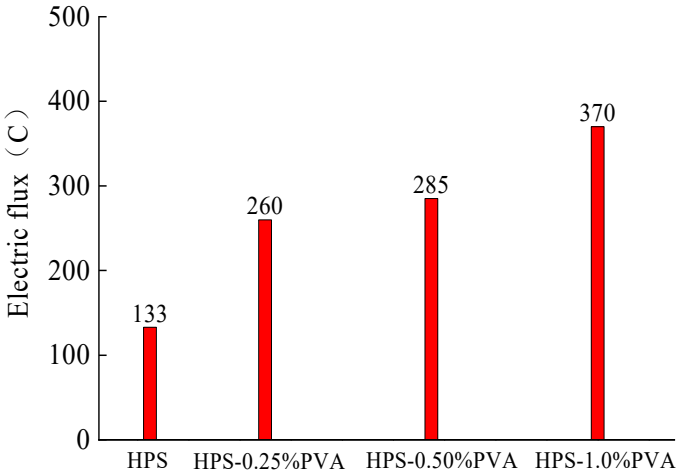

Figure 19. Electric flux of concrete with different PVA fiber contents.

As seen in the figure, the electrical flux of HPS with PVA fibers is higher than that of HPS without fibers, and the electrical flux increases with the increase in fiber content. The electric fluxes of HPS-0.25% PVA, HPS-0.50% PVA and HPS-1% PVA were 260C, 285C and 370C, respectively. This is because the incorporation of PVA fibers introduces more interfaces within the concrete, resulting in an increased number of pathways inside the concrete, which leads to a higher electrical flux. Further increasing the PVA fiber content reduces the fiber dispersion, leading to fiber agglomeration and uneven distribution within the concrete. This results in increased internal porosity, which further increases the electrical flux of HPS.

4.3. Carbonation Test

The variation curve of carbonation depth with curing age is shown in Figure 20. As shown in the figure, the carbonation depth of all mix proportion specimens gradually increases with the extension of the carbonation age. After 28 days of carbonation, the carbonation depth of all HPS mix specimens remained relatively small, ranging from 2.04 mm to 6.12 mm, which can be considered negligible. This indicates that high-performance shotcrete exhibits excellent durability. At the same curing age, the incorporation of PVA fibers increases the carbonation depth of HPS, and the higher the PVA fiber content, the greater the carbonation depth of the HPS. This is because the HPS matrix has a low water–binder ratio, and 15% silica fume is added, making the matrix relatively dense. The incorporation of PVA fibers introduces more interfaces within the concrete, leading to an increase in internal pathways. Due to the relatively low density of PVA fibers, a larger number of fibers are distributed per unit volume. As the PVA fiber content increases further, the fibers become more difficult to disperse uniformly within the matrix, reducing the density of the HPS, which is detrimental to its carbonation resistance. Previous studies have shown that the carbonation depth of concrete is closely related to time, and it can uniformly expressed as:

$$X_c = k_c\sqrt{t} \tag{21}$$

where X_c represents the carbonation depth of concrete, mm; k_c represents the carbonation coefficient, and $mm/d^{0.5}$; t represents the carbonation age, d.

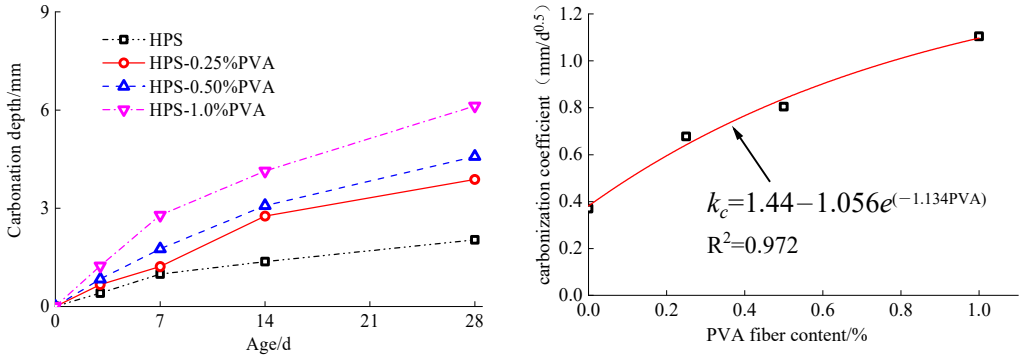

Figure 20. The impact of PVA fibers on the carbonation performance of HPS. (**a**) Carbonation depth and (**b**) carbonization coefficient.

Figure 20 shows the effect of PVA fiber content on the carbonation coefficient of HPS. Through analysis, it is evident that the carbonation coefficient exhibits an exponential relationship with the PVA fiber content.

Finally, the summarized carbonation depth prediction model for HPS is shown in Equation (22):

$$X_c = (1.44 - 1.056e^{(-1.134PVA)})\sqrt{t} \quad (22)$$

where PVA represents the volumetric content percentage of polyvinyl alcohol (PVA) expressed as a percentage (%).

More importantly, it is reported that ensuring appropriate number, spacing, and distribution of small entrained air bubbles in concrete is key to handling durability issues such as freeze–thaw and scaling, since the well-entrained air-void system provides empty chambers within the hydrated matrices to relieve the internal hydrostatic pressure driven by the expansion of water upon freezing.

However, the dense matrix structure of high-performance shotcrete (HPS) results in changes to the internal pore structure and void distribution due to the air trapped by the incorporated PVA fibers. This modification reduces the density of the shotcrete, causing high stresses in the void walls, ultimately leading to progressive microcracks and eventual spalling, which will alter its failure behavior under compression and negatively impact its impermeability. Consequently, the electrical flux and carbonation depth of HPS with fibers are higher than those of the reference group without fibers.

5. Conclusions

In this study, the effects of polyvinyl alcohol (PVA) fibers on the mechanical properties of high-performance shotcrete (HPS) were comprehensively evaluated. The research focused on various aspects, including compressive strength, splitting tensile strength, stress–strain behavior, constitutive modeling, and micro-mechanical properties. The following are the key findings of the study.

(1) The addition of PVA fibers greatly improved the splitting tensile strength of HPS, with the 0.50% dosage yielding the highest increases of 20.40%, 19.67%, and 30.77% at 1, 3, and 28 days, respectively. The 1.0% PVA fibers also enhanced ductility, as indicated by a 31.51% increase in peak strain.

(2) The incorporation of PVA fibers resulted in a reduction in compressive strength, peak compressive stress, and the elastic modulus of HPS. The peak stress and elastic modulus of HPS decreased with the addition of PVA fibers. For PVA fiber dosages of 0.25%, 0.50%, and 1.0%, the peak stress decreased by 21.35%, 17.93%, and 10.99%, and the compressive strength decreased by 15.11%, 10.44%, and 14.56%.

(3) PVA-HPS mixtures with different proportions exhibit excellent frost resistance, chloride ion penetration resistance, and carbonation resistance, with an electrical charge

being passed ranging from 133 to 370 C and the carbonation depths varying between 2.04 and 6.12 mm. On one hand, the incorporation of PVA fibers resulted in the reduced flowability of the mixture, leading to an increase in air void content within the HPS. As a result, the density of the matrix decreased, causing the electrical charge passed and average carbonation depth to increase with the rising fiber dosage. On the other hand, the randomly distributed PVA fibers effectively mitigate the damage and failure caused by freezing stresses on the shotcrete matrix. They help to eliminate the stress concentration at the tips of microcracks and alter the deflection direction of these microcracks, thereby enhancing the tensile performance of the matrix.

(4) The addition of PVA fibers effectively reduces microcrack formation and enhances the tensile strength and toughness of HPS. However, it also increases bubble volume and average bubble size, which negatively impacts compressive strength. Therefore, for optimal performance, a PVA fiber dosage of 0.25% to 0.5% is recommended. For ordinary shotcrete with a high water-to-binder ratio, trial spraying should be conducted based on design requirements and cost considerations to determine the appropriate dosage.

(5) Incorporating PVA fibers can markedly enhance the toughness of high-performance shotcrete (HPS) without significantly increasing its bulk density. This is particularly beneficial in complex service environments with high rock mass ratings, such as those encountered in the ongoing construction of the Sichuan–Tibet Railway in China. These environments are characterized by frequent seismic activity, collapses, landslides, debris flows, and other severe geological hazards like rock bursts in deep tunnels, high in situ stresses, and large deformations in soft rock. The addition of PVA fibers effectively improves the failure behavior of shotcrete and significantly extends its service life, making it a promising material with vast potential for future applications.

(6) Due to experimental limitations, the aspect ratio of the PVA fibers utilized in this study is fixed, and the durability tests primarily focus on the impact of a single factor. Future research could investigate the mechanical properties and coupling effects of various aspect ratios and hybrid fibers in conditions such as exposure to chloride salts, freeze–thaw cycles, and carbonation. This will offer more valuable insights into the use of PVA fibers in shotcrete applications within complex service environments.

Author Contributions: Conceptualization, G.Z. and K.L.; methodology, G.Z. and L.L.; validation, G.Z. and H.S.; formal analysis, G.Z. and L.L.; investigation, G.Z., C.C. and H.S.; Data curation, G.Z., L.L. and H.S.; Writing—original draft preparation, G.Z.; writing—review and editing, G.Z., K.L. and H.S.; funding acquisition, G.Z. All authors have read and agreed to the published version of the manuscript.

Funding: This research was funded by the Natural Science Foundation of Henan (grant number 242300421462), the Science and Technology Development Fund of the Yellow River Institute of Hydraulic Research (202112), the Excellent Young Talents Project of Yellow River Conservancy Commission (No. HQK-202310) and the Major Science and Technology Project of Henan Province (No. 231100320100).

Data Availability Statement: The original contributions presented in the study are included in the article, further inquiries can be directed to the corresponding author.

Conflicts of Interest: The authors declare no conflicts of interest.

Nomenclature

a	Ascend parameter	M	Meter
ASTM	American Society for Testing and Materials	MPa	Megapascal
$Al_2(SO_4)_3$	Aluminum Sulfate	MgO	Magnesium oxide
b	Descend parameter	N	Newton
C-S-H	Calcium Silicate Hydrate	nm	Nanometer
Cr	Relative Compressive Strength	PVA	Polyvinyl Alcohol

ECC	Engineered Cementitious Composites	PC	Portland cement
Er	Relative Dynamic Elastic Modulus	PTFE	Polytetrafluoroethylene
Fe_2O_3	Iron oxide	PAFRS	Polyamide Fiber-Reinforced Shotcrete
$g{\cdot}cm^{-3}$	Grams per Cubic Centimeter	Psi	Pound-force per square inch
K_2O	Potassium oxide	RTPF	Recycled Tire Polymer Fibers
kN	Sodium aluminate	Sr	Relative Splitting Tensile Strength
HPS	High-Performance Shotcrete	St	Steel
kcc	Coefficient of compressive strength	Xc	Carbonation depth
Kc	Equilibrium Constant	με	Micro strain
MPa	Megapascal	μW	Microwatt
MIP	Mercury intrusion porosimetry	%	Percentage

References

1. Raza, A.; Zhang, J.; Xu, S.; Umar, M.; Yuan, C. Experimental analysis of frost resistance and failure models in engineered cementitious composites with the integration of Yellow River sand. *Sci. Eng. Compos. Mater.* **2024**, *31*, 20240017. [CrossRef]
2. Yuan, C.; Raza, A.; Manan, A.; Ahmad, S.; Wang, C.; Umar, M. Experimental and FEM analysis on the impact of Yellow River Sand replacement rate on Engineered Cementitious Composite (ECC). *Proc. Inst. Civ. Eng.-Eng. Sustain.* **2024**. *ahead of print*. [CrossRef]
3. Zhang, Y.; Raza, A.; Umar, M.; Chen, Y.; Yuan, C. Study on Frost Resistance and Interface Bonding Performance through the Integration of Recycled Brick Powder in Ultra-High-Performance Concrete for Structural Reinforcement. *Materials* **2023**, *16*, 6999. [CrossRef]
4. Zhang, J.; Raza, A.; Fu, W.; Yuan, C. Research on uniaxial compression performance and constitutive relationship of RBP-UHPC after high temperature. *Sci. Eng. Compos. Mater.* **2024**, *31*, 20240011. [CrossRef]
5. Yuan, C.; Fu, W.; Raza, A.; Li, H. Study on Mechanical Properties and Mechanism of Recycled Brick Powder UHPC. *Buildings* **2022**, *12*, 1622. [CrossRef]
6. Memon, B.A.; Oad, M.; Buller, A.H.; Raza, A. Effect of Curing Methods on Tensile Strength of Green Concrete Cylinders Made with Demolishing Coarse Aggregates. *World J. Eng. Res. Technol.* **2020**, *6*, 66–75.
7. Hemphill, G.B. *Practical Tunnel Construction*; Jone Wiley Sons: Hoboken, NJ, USA, 2013; pp. 309–322. [CrossRef]
8. Colombo, M.; di Prisco, M.; Mazzoleni, L. Sprayed tunnel linings: A comparison between several reinforcement solutions. *Mater. Struct.* **2009**, *42*, 1295–1311. [CrossRef]
9. Hewlett, P.C. *Lea's Chemistry of Cement and Concrete*; Butterworth-Heinemann: London, UK, 2005; pp. 1053–1055. [CrossRef]
10. Massone Leonardo, M. Nazar Francisco Analytical experimental evaluation of the use of fibers as partial reinforcement in shotcrete for tunnels ils in Chile. *Tunn. Undergr. Space Technol.* **2018**, *77*, 13–25. [CrossRef]
11. Wang, J.; Niu, D.; Zhang, Y. Mechanical properties, permeability and durability of accelerated shotcrete. *Constr. Build. Mater.* **2015**, *95*, 312–328. [CrossRef]
12. Yun, K.K.; Kim, J.B.; Song, C.S.; Hossain, M.S.; Han, S. Rheological Behavior of High-Performance Shotcrete Mixtures Containing Colloidal Silica and Silica Fume Using the Bingham Model. *Materials* **2022**, *15*, 428. [CrossRef]
13. Yun, K.K.; Choi, S.Y.; Yeon, J.H. Effects of admixtures on the rheological properties of high-performance wet-mix shotcrete mixtures. *Constr. Build. Mater.* **2015**, *78*, 194–202. [CrossRef]
14. Wang, J.; Wang, T.; Zhang, Y.; Qian, X. Study on mechanical properties and self-sensing properties of sprayed high-performance concrete containing glass aggregate. *Front. Mater.* **2024**, *10*, 1320584. [CrossRef]
15. Lee, S.; Kim, D.; Ryu, J.; Lee, S.; Kim, J.; Kim, H.; Choi, M. An Experimental Study on the Durability of High Performance Shotcrete for Permanent Tunnel Support. *Tunn. Undergr. Space Technol.* **2006**, *21*, 431–436. [CrossRef]
16. Dickinson, R.M.; Afzal, M.F.U.D.; Mantawy, I.M.; Azizinamini, A. Non-proprietary ultra high-performance concrete mixtures for pneumatic spray applications. *Structures* **2024**, *60*, 105911. [CrossRef]
17. He, S.; Ma, W.; Cao, D.; Xia, B. Permanent Single-layer Tunnel Lining by Fibre-reinforced High Performance Shotcrete and Wet-mix Method. *Chin. J. Rock Mech. Eng.* **2004**, *23*, 35093517. [CrossRef]
18. Qian, H.; Umar, M.; Khan, M.N.A.; Shi, Y.; Manan, A.; Raza, A.; Chen, G. A State-of-the-Art Review on Shape Memory Alloys (SMA) in Concrete: Mechanical Properties, Self-Healing Capabilities, and Hybrid Composite Fabrication. *Mater. Today Commun.* **2024**, *40*, 109738. [CrossRef]
19. Shah, I.; Li, J.; Khan, N.; Almujibah, H.R.; Rehman, M.M.; Raza, A.; Peng, Y. Bond-Slip Behavior of Steel Bar and Recycled Steel Fibre-Reinforced Concrete. *J. Renew. Mater.* **2024**, *12*, 167–186. [CrossRef]
20. Cui, S.; Fu, F.; Zeng, G.; Chen, Z.; Li, G. Analysis on mechanical property and pore structure of concrete for spraying use in hot-dry environment fiber. *J. Southeast Univ. (Nat. Sci. Ed.)* **2022**, *52*, 43–49.
21. Wang, W.; Huo, J.; Zeng, L.; Liu, W.; Wang, Y. Interlayer Mechanical Characteristics and Anti-penetrability Performance of Combined Shotcrete in Single-shell Lining. *Mater. Rep.* **2023**, *37*, 90–96.
22. Kakooei, S.; Akil, H.M.d.; Jamshidi, M.; Rouhi, J. The effects of polypropylene fibers on the properties of reinforced concrete structures. *Constr. Build Mater* **2012**, *27*, 73–77. [CrossRef]

23. Zhang, P.; Li, Q. Effect of polypropylene fiber on durability of concrete compositecontaining fly ash and silica fume. *Compos. Part B Eng.* **2013**, *45*, 1587–1594. [CrossRef]
24. Bentegri, I.; Boukendakdji, O.; Kadri, E.-H.; Ngo, T.; Soualhi, H. Rheological andtribological behaviors of polypropylene fiber reinforced concrete. *Constr. Build. Mater.* **2020**, *261*, 119962. [CrossRef]
25. Monson, L.; Braunwarth, M.; Extrand, C.W. Moisture absorption by various polyamidesand their associated dimensional changes. *J. Appl. Polym. Sci.* **2008**, *107*, 355–363. [CrossRef]
26. Wang, J.; Dai, Q.; Si, R.; Guo, S. Investigation of properties and performances of Polyvinyl Alcohol (PVA) fiber-reinforced rubber concrete. *Constr. Build. Mater.* **2018**, *193*, 631–642. [CrossRef]
27. Şahmaran, M.; Özbay, E.; Yücel, H.E.; Lachemi, M.; Li, V.C. Frost resistance and microstructure of engineered cementitious composites: Influence of fly ash and micro poly-vinyl-alcohol fiber. *Cem. Concr. Compos.* **2012**, *34*, 156–165. [CrossRef]
28. Liu, G.; Cheng, W.; Chen, L. Investigating and optimizing the mix proportion of pumping wet-mix shotcrete with polypropylene fiber. *Constr. Build. Mater.* **2017**, *150*, 14–23. [CrossRef]
29. Guler, S.; Öker, B.; Akbulut, Z.F. Workability, strength and toughness properties of different types of fiber-reinforced wet-mix shotcrete. *Structures* **2021**, *31*, 781–791. [CrossRef]
30. Khooshechin, M.; Tanzadeh, J. Experimental and mechanical performance of shotcrete made with nanomaterials and fiber reinforcement. *Constr. Build. Mater.* **2018**, *165*, 199–205. [CrossRef]
31. Baricevic, M.; Pezer, M.; Rukavina, M.; Serdar, N.; Stirmer, N. Effect of polymer fibers recycled from waste tires on properties of wet-sprayed concrete. *Constr. Build. Mater.* **2018**, *176*, 135–144. [CrossRef]
32. Yang, J.-M.; Kim, J.-K.; Yoo, D.-Y. Performance of shotcrete containing amorphous fibers for tunnel applications. *Tunn. Undergr. Space Technol.* **2017**, *64*, 85–94. [CrossRef]
33. Jeon, J.K.; Kim, W.; Kim, G.Y.; Jeon, C.K. Polyamide Fiber Reinforced Shotcrete for Tunnel Application. *Materials* **2016**, *9*, 163. [CrossRef] [PubMed]
34. Yan, X.; Liu, L.; Zhang, J.; Li, Y.; Wang, H. Experimental study on basic mechanical properties of steel fiber-reinforced siliceous wet shotcrete. *Adv. Mater. Sci. Eng.* **2018**, *4*, 1–8. [CrossRef]
35. Jeng, F.; Lin, M.-L.; Yuan, S.-C. Performance of toughness indices for steel fiber reinforced shotcrete. *Tunn. Undergr. Space Technol.* **2002**, *17*, 69–82. [CrossRef]
36. Liu, X.; Li, Q.; Li, J. Shrinkage and mechanical properties optimization of spray-based 3D printed concrete by PVA fiber. *Mater. Lett.* **2022**, *319*, 132253. [CrossRef]
37. Xu, H. Optimization Design and Performance Study of Sprayable High Performance Concrete for Secondary Lining of Tunnel. Master's Thesis, Southeast University, Nanjing, China, 2022.
38. Huang, B.-T.; Li, Q.-H.; Xu, S.-L.; Zhou, B. Strengthening of reinforced concrete structure using sprayable fiber-reinforced cementitious composites with high ductility. *Compos. Struct.* **2019**, *220*, 940–952. [CrossRef]
39. Yu, Z.J.; Lee, M.H.; Yun, H.D. Mechanical Properties of Sprayable Fiber Reinforced Strain-Hardening Cement Composite (SHCC). *Appl. Mech. Mater.* **2014**, *372*, 211–214. [CrossRef]
40. Xu, S.; Zhou, B.; Li, Q.; Wu, Y. Mechanical performance of sprayable Ultra High Toughness Cementitious Composites. *Shuili Xuebao* **2015**, *46*, 619–625. [CrossRef]
41. Fantilli, A.P.; Mihashi, H.; Nishiwaki, T. Tailoring hybrid strain-hardening cementitious composites. *ACI Mater. J.* **2014**, *111*, 211–218. [CrossRef]
42. Kim, Y.Y.; Fischer, G.; Lim, Y.M.; Li, V.C. Mechanical Performance of Sprayed Engineered Cementitious Composite Using Wet-Mix Shotcreting Process for Repair Applications. *ACI Mater. J.* **2004**, *101*, 42–49. [CrossRef]
43. Yun, K.-K.; Choi, P.; Yeon, J.H. Microscopic investigations on the air-void characteristics of wet-mix shotcrete. *J. Mater. Res. Technol.* **2019**, *8*, 1674–1683. [CrossRef]
44. Talukdar, S.; Heere, R. The effects of pumping on the air content and void structure of air-entrained, wet mix fibre reinforced shotcrete. *Case Stud. Constr. Mater.* **2019**, *11*, e00288. [CrossRef]
45. Choi, P.; Yeon, J.H.; Yun, K.-K. Air-void structure, strength, and permeability of wet-mix shotcrete before and after shotcreting operation: The influences of silica fume and air-entraining agent. *Cem. Concr. Compos.* **2016**, *70*, 69–77. [CrossRef]
46. Zeng, L.; Zhao, S.; Wang, W.; Qiao, M.; Mu, S.; Ran, Q.; Hong, J.; Hu, M. Air-void Structure Characteristics, Water Penetration Resistance and Freeze-thaw Resistance of Hardened Shotcrete. *J. Chin. Ceram. Soc.* **2020**, *48*, 1781–1790.
47. Zhang, G.; An, M.; Wang, Y. Research on Freeze-thaw Resistance and Air-void Structure Characteristics of High-Performance Wet-Mix Shotcrete. *J. China Railw. Soc.* **2023**, *45*, 151–157. [CrossRef]
48. *JGJ/T 372-2016*; Technical Specification for Application of Sprayed Concrete. China Architecture & Building Press: Beijing, China, 2016.
49. Yuan, C.; Xu, S.; Raza, A.; Wang, C.; Wang, D. Influence and Mechanism of Curing Methods on Mechanical Properties of Manufactured Sand UHPC. *Materials* **2022**, *15*, 6183. [CrossRef] [PubMed]
50. Raza, A.; Memon, B.A.; Oad, M. Effect of Curing Types on Compressive Strength of Recycled Aggregates Concrete. *Quaid-E-Awam Univ. Res. J. Eng.* **2019**, *17*, 7–12. [CrossRef]
51. Yuan, C.; Feng, H.; Raza, A.; Shen, L.; Sun, Y.; Zhang, C.; Wang, B.; Wu, X.; Chen, N.; Sun, G. Ultra-High-Performance Concrete with Waste Brick Powder and Preparation Method and Application Thereof. U.S. Patent US11905213B2, 20 February 2024.

52. *GB/T50081-2019*; Standard for Test Methods of Concrete Physical and Mechanical Properties. China Architecture & Building Press: Beijing, China, 2019.
53. Yu, Z.; Zhao, H.; An, M.; Liu, Y. Mechanical Properties of Reactive Powder Concrete under Triaxial Compression. *J. China Railw. Soc.* **2017**, *39*, 117–122. [CrossRef]
54. *ASTM C457/C457M-16*; Standard Test Method for Microscopical Determination of Parameters of the Air-Void System in Hardened Concrete. ASTM International: West Conshohocken, PA, USA, 2016.
55. Razzak, A.; Memon, B.A.; Oad, M.; Raza, A. Effects of height to diameter ratio on compressive strength of recycled aggregate concrete. *QUEST Res. J.* **2020**, *18*, 60–65.
56. Yuan, C.; Zhang, J.; Raza, A.; Fu, W. Residual and damage properties of recycled brick powder-UHPFRC after high temperature. *Proc. Inst. Civ. Eng.-Constr. Mater.* **2024**. *Ahead of Print*. [CrossRef]
57. *GB/T 50082-2024*; Standard for Test Methods of Long-Term Performance and Durability of Concrete. Ministry of Housing and Urban-Rural Development: Beijing, China, 2024.
58. Cengiz, Ö.; Turanlı, L. Comparative evaluation of steel mesh, steel fibre, and high-performance polypropylene fiber reinforced shotcrete in panel test. *Cem. Concr. Res.* **2004**, *34*, 1357–1364. [CrossRef]
59. Xu, Y.; Xing, G.; Huang, J.; Wu, X.; Lu, Y. Effect of PVA Fiber and Carbon Nanotubes Modification on Mechanical Properties of Concrete. *J. Build. Mater.* **2023**, *26*, 809–815+822. [CrossRef]
60. Zhao, Y.; Wang, Z.; Wang, L.; Fan, X. Grey Entropy Analysis of Macro and Micro Properties of BFRC after Freeze-Thaw Cycles. *J. Build. Mater.* **2019**, *22*, 45–53. [CrossRef]
61. Hu, Z.; Ding, H.; Lai, J.; Wang, H.; Wang, X.; He, S. The durability of shotcrete in cold region tunnel: A review. *Constr. Build. Mater.* **2018**, *185*, 670–683. [CrossRef]
62. Chen, J.; Zhao, X.; Luo, Y.; Deng, X.; Liu, Q. Investigating freeze-proof durability of C25 shotcrete. *Constr. Build. Mater.* **2014**, *61*, 33–40.
63. Yang, C.; Liu, F.; Pan, Y.; Li, K. Mechanical properties of polyvinyl alcohol fiber-reinforced rapid-setting concrete under freeze-thaw cycles. *J. Southeast Univ. (Nat. Sci. Ed.)* **2019**, *49*, 334–339.
64. Liu, S.; Yin, L.; Yan, C.; Zhang, J.; Yan, M. Effects of polyvinyl alcohol fibers on the flexural strength of salt-frozen concrete. *Mater. Rep.* **2015**, *29*, 92–97.
65. Huang, B.T.; Wu, J.; Yu, J.; Dai, J.G.; Leung, C.K.; Li, V.C. Seawater sea-sand engineered/strain-hardening cementitious composites (ECC/SHCC): Assessment and modeling of crack characteristics. *Cem. Concr. Res.* **2021**, *140*, 106292. [CrossRef]